L2O- g^{\dagger} : Learning to Optimize Parameterized Quantum Circuits with Fubini–Study Metric Tensor

Yu-Chao Huang^{1,*} and Hsi-Sheng Goan^{1,2,3,†}

¹Department of Physics and Center for Theoretical Physics, National Taiwan University, Taipei 106319, Taiwan ²Center for Quantum Science and Engineering, National Taiwan University, Taipei 106319, Taiwan ³Physics Division, National Center for Theoretical Sciences, Taipei 106319, Taiwan (Dated: July 25, 2024)

Before the advent of fault-tolerant quantum computers, variational quantum algorithms (VQAs) play a crucial role in noisy intermediate-scale quantum (NISQ) machines. Conventionally, the optimization of VQAs predominantly relies on manually designed optimizers. However, learning to optimize (L2O) demonstrates impressive performance by training small neural networks to replace handcrafted optimizers. In our work, we propose $L2O-g^{\dagger}$, a quantum-aware learned optimizer that leverages the Fubini-Study metric tensor (g^{\dagger}) and long short-term memory networks. We theoretically derive the update equation inspired by the lookahead optimizer and incorporate the quantum geometry of the optimization landscape in the learned optimizer to balance fast convergence and generalization. Empirically, we conduct comprehensive experiments across a range of VQA problems. Our results demonstrate that $L2O-g^{\dagger}$ not only outperforms the current SOTA hand-designed optimizer without any hyperparameter tuning but also shows strong out-of-distribution generalization compared to previous L2O optimizers. We achieve this by training $L2O-g^{\dagger}$ on just a single generic PQC instance. Our novel quantum-aware learned optimizer, $L2O-g^{\dagger}$, presents an advancement in addressing the challenges of VQAs, making it a valuable tool in the NISQ era. The implementation and data are available at: https://github.com/Physics-Morris/L2O-g.

I. INTRODUCTION

Quantum computers provide a different paradigm of computing based on quantum mechanical principles such as superposition and entanglement. It has the potential to change the future of computing [19, 66]. However, a reliable quantum computer for tasks like factoring large numbers requires 10⁶ qubits and a probability of error per quantum gate of the order of 10^{-6} [54]. Currently, we have around 10^2 qubits and an error rate between 10^{-2} and 10^{-4} [1]. Before the advent of the first fault-tolerant quantum computer, noisy intermediate-scale quantum (NISQ) computing [55] with hundreds of qubits could potentially surpass classical computing. In particular, variational quantum algorithms (VQAs) emerge as crucial algorithms for NISQ devices [15]. In essence, VQAs consist of a parameterized quantum circuit (PQC) and use a classical computer to optimize the cost function based on the output of the quantum computer (see Figure 2). Applications include many-body quantum physics [33], chemistry [46], combinatorial optimization [22, 45], and machine learning [10, 64].

However, it remains uncertain whether VQAs can surpass classical computers in the NISQ era as they scale up. On the classical optimization side, Bittel and Kliesch [12] show that even if quantum systems are classically tractable (e.g., logarithmic qubits or free fermions), classical optimization remains NP-hard. Furthermore, in-

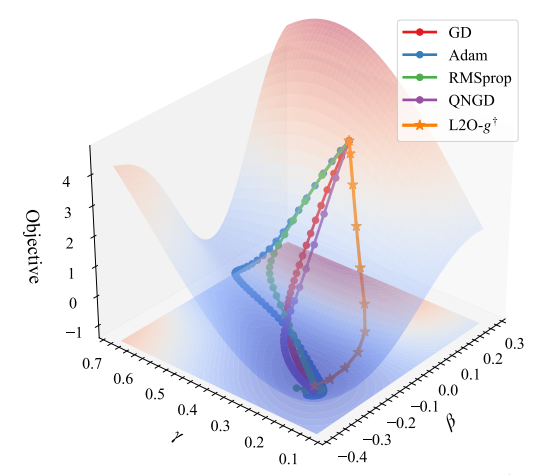


FIG. 1: A Motivating Toy Example of L2O- g^{\dagger} Optimizing MaxCut Problem with QAOA ($V=5, p=0.9, p_{\mathbf{layer}}=1$). L2O- g^{\dagger} automatically adjusts step size approaching the minimum and converges to the minimum with only a few steps.

creasing the expressiveness of the variational ansatz often leads to trainability issues like barren plateaus and narrow gorges [16]. McClean et al. [47] show that the exponential vanish of the gradient with the number of qubits makes it untrainable. To circumvent the problem, there are three active areas: parameters initialization technique [26, 79], circuit design [15, 27, 40], and optimization technique [24, 37, 43, 63, 68]. L2O- g^{\dagger} falls into the last category, L2O- g^{\dagger} improving the optimization with an auto-adjustable training strategy consisting of a quantum-aware learned optimizer (see toy example in Figure 1).

^{*} r11222015@ntu.edu.tw

[†] goan@phys.ntu.edu.tw

When optimizing a PQC in VQAs, we usually use a hand-designed analytical algorithm. Additionally, most optimizer requires a careful choice of optimizer and global search for hyperparameters given different optimizing problems. To address this issue, learning to optimize (L2O) uses a small neural network to replace the hand-crafted optimizer to learn the optimal optimization strategy tailored for a similar distribution of tasks, and dynamically adjust during the optimization process. This approach leverages the intuition of a neural network as a universal function approximator [29].

Leaned optimizer was introduced by Andrychowicz et al. [4] which uses a coordinate-wise LSTM to replace hand-crafted optimizer. Their results show faster convergence compared to hand-crafted optimizers on similar classes of optimization problems in their training sets. Inherit the same architecture from Andrychowicz et al. [4], Verdon et al. [71] and Wilson et al. [73] demonstrate the simple LSTM learned optimizer's ability to tackle the problem of optimizing VOAs under limited scenarios away from the training distribution. However, No Free Lunch Theorem [53] suggest there is no single optimizer that trumps others on every objective. Therefore, we set out to address the generalizability problem of previous purely classical learned optimizers by replacing the hand-designed optimizer with a quantum-aware learned optimizer tailored to tackle optimization in VQAs.

In this work, we propose a quantum-aware learned optimizer, L2O- g^{\dagger} , which dynamically adjusts the balance between parameter space optimization and distribution space optimization during the optimization process. We theoretically derive the update equation to incorporate the quantum geometry of the parameter space in the learned optimizer, using the Fubini-Study metric tensor along with learned update directions and update steps to effectively balance fast convergence and generalization across different VQAs. Specifically, a learnable vector balances the parameter space and distribution space optimization coordinate-wise. We show that L2O- g^{\dagger} generalizes to all kinds of optimization problems in VQAs by training on a single generic PQC instance. Without any hyperparameter tuning, it matches or surpasses a hyperparameter-tuned hand-crafted optimizer in optimizing a wide variety of VQAs. Limitations of our work are discussed in Section VII.

A. Contributions

Our contributions are summarized as follows:

- We propose L2O- g^{\dagger} with theoretical motivation and empirically demonstrate its robustness against a diverse array of optimization problems in VQAs.
- We show that L2O- g^{\dagger} can generalize well to a wide range of VQAs problems by training on a single generalized PQC instance.

• We open source our implementation, experiments data, and results for minimum effort integration of any future VQAs problems with L2O-g[†].

B. Notation

We denote the set $[n] := \{1, \ldots, n\}$. We denote vectors in lowercase bold letters and matrices in uppercase bold letters. The Pauli matrices are denoted by $\hat{\sigma}_x$, $\hat{\sigma}_y$, and $\hat{\sigma}_z$. The operator norm of an operator \hat{X} is denoted by $\|\hat{X}\|$. The ℓ_2 -norm of a vector \mathbf{x} is denoted by $\|\mathbf{x}\|_2$. The inner product of vectors \mathbf{x} and \mathbf{y} is denoted by $\langle \mathbf{x}, \mathbf{y} \rangle$. The element-wise product of vectors \mathbf{x} and \mathbf{y} is denoted by $\mathbf{x} \circ \mathbf{y}$ and element-wise application of a function f to a vector \mathbf{x} is denoted by $f[\mathbf{x}]$.

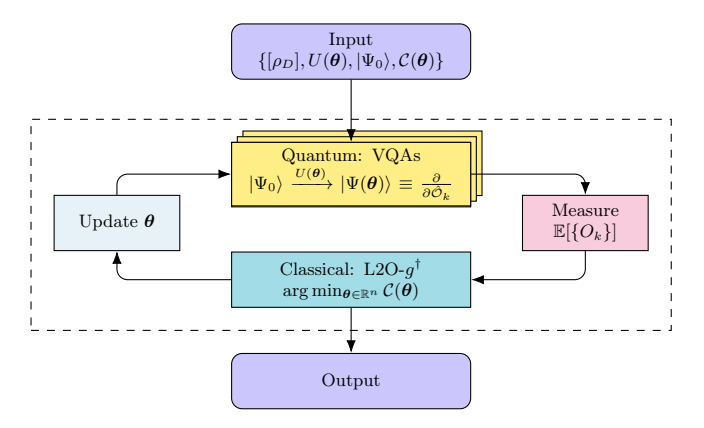


FIG. 2: Schematic Diagram for Variational Quantum Algorithms. In classical optimization, we use L2O- g^{\dagger} to find the optimal parameters θ^* for the given cost function $C(\theta)$. L2O- g^{\dagger} iteratively updates the parameter θ until it converges to an approximate solution.

II. THEORETICAL MOTIVATION

In this section, we provide the theoretical motivation for L2O- g^{\dagger} , a quantum-aware learned optimizer that balances fast convergence and generalization. We first introduce the relevant mathematical formulation of the mirror descent framework. Extending the concept of optimization geometric of parameter space, we add the additional regularization term for penalized moving too far away from the direction of gradient to effectively balance convergence and generalization. This approach incorporates the geometry of the parameter space into the learned optimizer, differentiating it from previous works that used purely classical learned optimizers [71, 73]. Specifically, we use a learnable vector that acts coordinate-wise on all the parameters θ , dynamically controlling convergence speed and generalization during the optimization process. adjusted by the types of VQA problems.

To accommodate the geometry of the optimization landscape, the mirror descent framework allows us to incorporate a generic distance function. The update equation has the following form:

$$\theta_{t+1} \leftarrow \arg\min_{\theta} \left\{ \langle \theta, \nabla \mathcal{C}(\theta_t) \rangle + D_{\Phi}(\theta, \theta_t) \right\}$$
 (1)

where D_{Φ} is the Bregman divergence to some function $\Phi : \mathbb{R} \to \mathbb{R}$ defined as:

$$D_{\Phi}(\theta, \theta_t) = \Phi(\theta) - \Phi(\theta_t) - \langle \nabla \Phi(\theta_t), \theta - \theta_t \rangle. \tag{2}$$

For example, if we choose $D_{\Phi}(\theta, \theta_t) = \frac{1}{2} \|\theta - \theta_t\|_2^2$, it results in the gradient descent algorithm. Alternatively, if we choose $D_{\Phi}(\theta, \theta_t) = \frac{1}{2} \|\theta - \theta_t\|_2^2 + \beta \sum_{i=1}^t \|\theta - \theta_i\|_2^2$ it corresponds to the momentum optimizer. Finally, if we let $D_{\Phi}(\theta, \theta + d\theta) = \text{KL}(\theta \|\theta + d\theta)$, where KL represents the Kullback-Leibler divergence, it becomes the Quantum Natural Gradient [68] in the Mirror Descent framework:

$$\theta_{t+1} \leftarrow \arg\min_{\theta} \left\{ \langle \boldsymbol{\theta}, \nabla \mathcal{C}(\theta_t) \rangle + \frac{1}{2\eta} \|u\|_{g(\theta_t)}^2 \right\}$$
 (3)

where $\mathbf{u} = (\theta - \theta_t)$ and $\|u\|_{g(\theta_t)}^2 := \langle u, g(\theta_t)u \rangle$ and g_{ij} is the Fubini-Study metric tensor define as:

$$g_{ij} = \operatorname{Re} \left(\langle \partial_i \psi | \partial_j \psi \rangle - \langle \partial_i \psi | \psi \rangle \langle \psi | \partial_j \psi \rangle \right). \tag{4}$$

In Equation (3), the first term is the linear approximation of \mathcal{C} at $\boldsymbol{\theta}_t$ that is $\mathcal{C}(\boldsymbol{\theta}) \approx \mathcal{C}(\boldsymbol{\theta}_t) + \langle \boldsymbol{\theta} - \boldsymbol{\theta}_t, \nabla \mathcal{C}(\boldsymbol{\theta}_t) \rangle$. The second term $\frac{1}{2\eta} \|u\|_{g(\theta_t)}^2$ is the regularizer term penalized $\boldsymbol{\theta}$ moving too far away from $\boldsymbol{\theta}_t$ modified by metric tensor $g(\boldsymbol{\theta}_t)$. We add an additional regularizer term as $\frac{\gamma_2}{2\eta} \|u - v\|_{g(\theta_t)}^2$ to penalized $\boldsymbol{\theta}$ moving too far away from $\boldsymbol{\theta}_t - \nabla \mathcal{C}(\boldsymbol{\theta}_t)$ modified by metric tensor $g(\boldsymbol{\theta}_t)$. We control the two regularizer terms with parameters γ_1 and γ_2 . With the addition of new regularizer terms, it provides the following update equation:

$$\theta_{t+1} \leftarrow \arg\min_{\theta} \left\{ \langle \theta, \nabla \mathcal{C}(\theta_t) \rangle + \frac{\gamma_1}{2\eta} \|u\|_{g(\theta_t)}^2 + \frac{\gamma_2}{2\eta} \|u - v\|_{g(\theta_t)}^2 \right\}$$
(5)

where $\mathbf{v} = -\nabla \mathcal{C}(\theta_t)$, and $\gamma_1 > 0, \gamma_2 > 0$ are parameters that modulate between two regularizers. The modified gradient given by the optimization problem in Equation (5) is

$$\nabla \widetilde{\mathcal{C}}(\theta) = \left(\frac{\gamma_1}{\gamma_1 - \gamma_2} g^{\dagger} - \frac{\gamma_2}{\gamma_1 - \gamma_2} I\right) \boldsymbol{v}. \tag{6}$$

III. METHODOLOGY

A. Background and Problem Formulation

A parameterized quantum circuit $U(\boldsymbol{\theta})$ has parameters $\boldsymbol{\theta} \in \Theta \subseteq \mathbb{R}^N$. To enhance the expressibility of VQAs,

 $U(\boldsymbol{\theta})$ usually consists of l layers of unitaries:

$$U(\boldsymbol{\theta}) = U_l(\boldsymbol{\theta}_l) \cdots U_2(\boldsymbol{\theta}_2) U_1(\boldsymbol{\theta}_1), \tag{7}$$

where θ_l is the *l*-th layers of θ . Each unitary can be written as

$$U_l(\boldsymbol{\theta}_l) = \prod_m e^{-i\theta_m \hat{H}_m} W_m \tag{8}$$

where H_m is Hermitian operator and W_m is an unparameterized unitary. For example, QAOA with p layers has the following unitary form $U_l(\boldsymbol{\alpha}_l,\boldsymbol{\beta}_l)=e^{-i\beta_l\hat{H}_M}e^{-i\gamma_l\hat{H}_C}$, where \hat{H}_C is the cost Hamiltonian, \hat{H}_M is the mixer Hamiltonian, and the respective parameters are $\boldsymbol{\gamma} \in \mathbb{R}^p$ and $\boldsymbol{\beta} \in \mathbb{R}^p$. The cost function encode by VQAs is some observable \hat{H} in terms of parameters $\boldsymbol{\theta}$ define as:

$$C(\boldsymbol{\theta}) = \langle \psi_0 | U^{\dagger}(\boldsymbol{\theta}) \hat{H} U(\boldsymbol{\theta}) | \psi_0 \rangle, \tag{9}$$

with the initial state $|\psi_0\rangle$ on N_q qubits. Parameter usually initialize with ground state $|0\rangle^{\otimes N_q}$ or other heuristic strategies [34, 39]. Given sample ρ_d from dataset of training state $[\rho_D]$. The objective for VQAs problem is finding the optimal parameters θ^* such that

$$\boldsymbol{\theta}^* = \arg\min_{\boldsymbol{\theta} \in \mathbb{R}^n} \sum_{\rho_d \in [\rho_D]} \mathcal{C}_{\rho_d}(\boldsymbol{\theta}). \tag{10}$$

The overview diagram for VQAs is illustrated in Figure 2. VQA is a hybrid framework consisting of a parameterized quantum circuit and leverages a classical computer to iteratively update the parameters $\boldsymbol{\theta}$ until it converges. However, training a PQC with a classical optimizer to find the optimal parameters $\boldsymbol{\theta}^*$ is generally an NP-hard problem [12]. A common-use algorithm is the descent algorithm which can be written as a general form

$$x_{k+1} = x_k + t_k \Delta x_k \tag{11}$$

which produce a optimization trajectory $[x_k]$. A natural choice is setting $\Delta x = -\nabla f(x)$, and it leads to the gradient descent algorithm. However, hand-designed optimizers critically depend on the choice of hyperparameters. To tackle this issue, learning to optimize (L2O) has provided a new paradigm by training a small neural network to "learn" the update rule, leveraging the neural network's capacity as a universal function approximator [29]. Another major challenge for the trainability of VQAs is barren plateaus and narrow gorges in PQCs cost function landscape [5, 47]. The variance of gradient respect with any $\theta_{\mu} \in \theta$ vanishes exponentially with the number of qubits N_q :

$$Var_{\boldsymbol{\theta}}[\partial_{\mu}\mathcal{C}](\boldsymbol{\theta}) < F(N_a) \tag{12}$$

with $F(N_q) \in \mathcal{O}(b^{-N_q})$ for some constant b > 1.

In L2O- g^{\dagger} , we replace $t_k \Delta x_k$ with a quantum-aware Long Short-Term Memory Model denote as L2O- g^{\dagger} . L2O- $g^{\dagger}(\cdot;\phi)$ is a parametric update function with metaparameters $\phi \in \Phi$ which takes the input state z_t then

update PQC parameter to θ_{t+1} . The corresponding update equation analogy to Equation (11) is given by the following parameter update rule

$$\boldsymbol{\theta}_{t+1} = \boldsymbol{\theta}_t - L2O - g^{\dagger}(\boldsymbol{z}_t; \boldsymbol{\phi}). \tag{13}$$

The goal of VQAs is to minimize the expected loss for cost function \mathcal{C} at k-step which we define as $L_k(\boldsymbol{\theta}) = \mathbb{E}_{\rho_d}[\mathcal{C}_{\rho_d}(\boldsymbol{\theta}_k)]$. The objective for L2O- g^{\dagger} is find optimal $\boldsymbol{\phi}^*$ that minimize the outer-loss $\mathcal{L}(\boldsymbol{\phi};T)$,

$$\mathcal{L}(\phi; T) = \sum_{t=1}^{T} w_t L_t(\boldsymbol{\theta}_t), \quad \phi^* = \arg\min_{\boldsymbol{\phi} \in \Phi} \mathcal{L}(\boldsymbol{\phi}; T) \quad (14)$$

where w_t is weighted term and T is the horizon for trajectory.

B. L2O- q^{\dagger} Architecture

In this section, based on our theoretical motivation in Section II. We propose L2O- g^{\dagger} , a quantum-aware learned optimizer that dynamically balances between convergence speed and generalization. In Figure 1 gives a toy example of L2O- g^{\dagger} on optimizing the MaxCut problem with QAOA. The optimization trajectory learned by L2O- g^{\dagger} exhibits totally different strategy compared with any first-order and second-order optimizer. It dynamically adjusts step size and converges to a minimum with only a few steps.

We describe the overall architecture of our quantum-aware learned optimizer in this section. Figure 3 illustrates the architecture of our proposed method. It consists of a learned optimizer, a recurrent neural network with parameters $\phi \in \Phi$. The input state $z_t = (\log(|\nabla|), \operatorname{sgn}(\nabla))$ follows the method by Andrychowicz et al. [4]. It returns the parameter update for the optimizee, a parameterized quantum circuit. We summarize the entire L2O- q^{\dagger} as a function:

$$\alpha_t, \beta_t, \gamma_t, h_t, c_t = \text{L2O-}g^{\dagger}(\boldsymbol{z_t}, h_{t-1}, c_{t-1})$$
 (15)

where h_t and c_t are the hidden state and cell state of the Long Short-Term Memory model at time step t. It outputs the update step $\eta_t = \exp\left[\lambda_b \alpha_t\right] \in \mathbb{R}^N$ and the update direction $v = \lambda_a \beta_t \in \mathbb{R}^N$ which act coordinatewise on each parameter θ in PQC. The scale factor are $\lambda_a = \lambda_b = 0.01$.

Inspired by Equation (6), we replace γ_1 and γ_2 with a coordinate-wise learnable vector $\gamma_t \in (0,1)^N$, defined as $\gamma_t = \text{Sigmoid}(\text{Linear}(h_t))$. It modulates the balance between two terms expressed as $\nabla \widetilde{\mathcal{C}}(\theta_t) = \left((1-\gamma_t)g_t^{\dagger} + \gamma_t I\right)v$ where $B_t = \left((1-\gamma_t)g_t^{\dagger} + \gamma_t I\right)$ acts as a effective preconditioner. It combines the update direction modified by the parameter space and the distribution space controlled by the learnable vector γ that auto-adjusts during the optimization process. Combining all, it gives us the updated equation for L2O- q^{\dagger} :

$$\boldsymbol{\theta}_{t+1} = \boldsymbol{\theta}_t - \boldsymbol{\eta}_t \circ \boldsymbol{B}_t \boldsymbol{v}_t \tag{16}$$

where B_t is a diagonal matrix.

C. Training Details

Learned optimizers are known to be unstable and difficult to train [48]. Backpropagation through unrolled optimization can result in a strong bias for short truncations or exploding norms for long truncations. Therefore, we adopt the curriculum learning technique for the learned optimizer proposed by Chen et al. [17]. It gradually increases the difficulty of the problem to facilitate faster convergence, better generalization, and stable training. In $\text{L2O-}g^{\dagger}$, the unrolled length gradually increases in this sequence: $T_{\text{unrolled}} = [10, 20, 40, 60, 80, \ldots]$. When training steps are at the i^{th} stage, the validation length mismatches at the $(i+1)^{\text{th}}$ stage. Training terminates when none of the validation losses at the $(N+1)^{\text{th}}$ stage is lower than the N^{th} stage-trained model.

In the following experiment detailed in Section IV. We train two models, each using a single PQC as training data: a generic PQC for solving VQE and QML tasks, and a QAOA circuit for MaxCut and Sherrington-Kirkpatrick Model tasks.

D. Baseline Optimizers

There is a collection of hand-designed optimizers [61] for optimizing high-dimensional and non-convex deep learning models. In our experiments, we select several popular optimizers, including RMSprop [28], Adam [36], Gradient Descent, Quantum Natural Gradient Descent [68], Momentum [60], and Adagrad [21].

IV. EXPERIMENTS

In this section, we benchmark L2O- g^{\dagger} on a broad spectrum of VQA problems. Our experiments can organized into the following three parts, respectively showing:

- L2O-g[†] can optimize general parameterized quantum circuits by training on a single instance, and it surpasses the hand-design optimizer in terms of convergence speed.
- By training L2O- g^{\dagger} on a single general PQC, it can tackle all kinds of real VQAs problems including VQE for chemistry, QAOA for MaxCut and Sherrington-Kirkpatrick Model, and QML for data-reuploading circuits (see Sections IV A to IV E). Additionally, out-of-box L2O- g^{\dagger} can match or out-perform hyperparameter tuned optimizer.
- Conducting ablation study on various parts of L2O- g^{\dagger} , and show that it surpasses previous learned optimizer baselines for optimizing PQC on generalizability and convergence speed (see Section IV F).

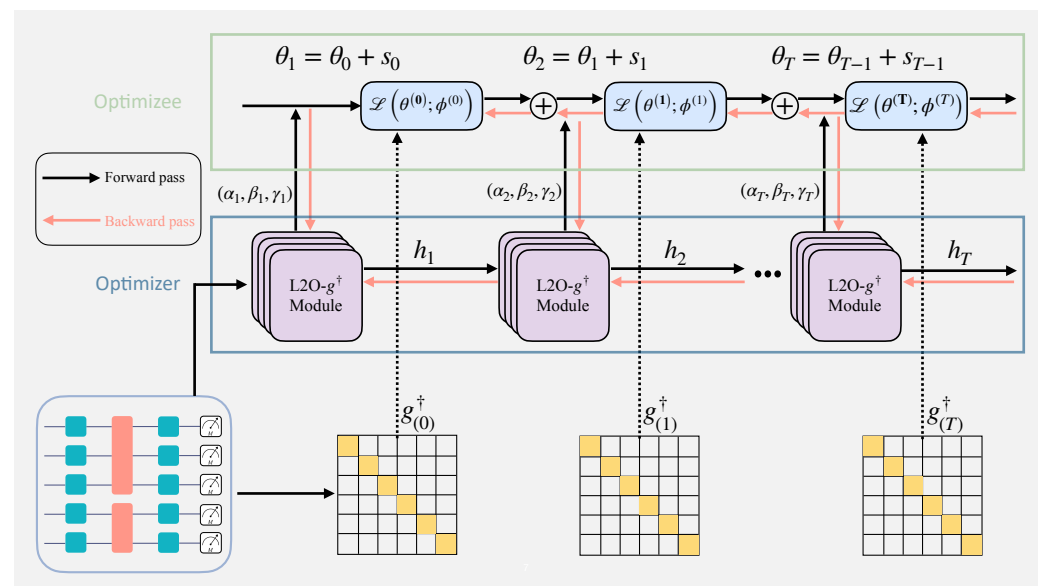


FIG. 3: Overall Architecture of Quantum-Aware Learned Optimizer L2O- g^{\dagger} . Given the parameters θ_t from PQC, L2O- g^{\dagger} dynamically balances between distribution space optimization and parameter space optimization using the learning strategy learned by the L2O- g^{\dagger} module. The L2O- g^{\dagger} module consists of a recurrent neural network, and the output values pass through a linear layer, returning three vectors $(\boldsymbol{\alpha}_t, \boldsymbol{\beta}_t, \boldsymbol{\gamma}_t)$ at the time step t in the optimizee trajectory $[x_T]$. The output for distribution space optimization is modified by the Fubini-Study metric tensor g^{\dagger} . Along with the update step $\eta_t = \exp[\lambda_b \alpha_t] \in \mathbb{R}^N$ and the update direction $v = \lambda_a \beta_t \in \mathbb{R}^N$, these update the parameters to θ_{t+1} . In the forward pass, the L2O- g^{\dagger} module takes the hidden state h_t , cell state c_t , and pre-processed input state c_t . The backward pass happens after every $T_{\text{unrolled}}^{(i)}$ at the i-stage of curriculum learning, where it gradually increases to facilitate exploration and exploitation.

- a. Tasks Setting. The tasks setting overview are the following:
 - Random Parameterized Quantum Circuit (see Section IV A): Farhi et al. [22] used it to showcase the effect of the barren plateau. We follow the same experimental setup in Stokes et al. [68] for the baseline optimizer.
 - VQE [52] for Chemistry (see Section IVB): We implement various ansatz including Hardware Efficient Ansatz (HEA) and $U_{\text{ent}}^{(1)}$ ansatz [9], Unitary Coupled-Cluster Singles and Doubles (UCCSD) ansatz [9] and calculate various ground states of molecules including H₂, H₃⁺, H₄, LiH, BeH₂, and H₂O.
 - QAOA [22] for MaxCut (see Section IV C): We calculate the approximation ratio by QAOA for the MaxCut problem with randomly generated Erdős-Rényi graphs and compare it with learning rate grid search quantum natural gradient descent algorithm [68].
 - QAOA [22] for Sherrington-Kirkpatrick Model (see Section IV D): We compare the final objective value for a wide variety of optimizers for optimizing the Sherrington-Kirkpatrick model with QAOA of various layers $p_{\rm layer}$.
 - QML [11] for Data Re-upload Circuit [57] (see Section IV E): We implement the same experimental

setup from Pérez-Salinas et al. [57] and compare a single trial L2O- g^{\dagger} with second-order optimizer L-BFGS-B and learning rate tuned Adam and Momentum.

A. Random Parameterized Quantum Circuit

a. Setup. We employ the circuit design in McClean et al. [47]. It consists of: Initialized with $|\psi_1\rangle=(R_Y(\frac{\pi}{4})^{\otimes N_q})\,|0\rangle^{\otimes N_q},$ then followed by l layers given by $|\psi_l\rangle=(U_{\rm CZ}^{(l)}U_{\rm P}^{(l)})\cdots(U_{\rm CZ}^{(1)}U_{\rm P}^{(1)})\,|\psi_1\rangle.$ In particular, $U_{\rm P}^{(i)}=\bigotimes_{j=1}^n R_{P_j}(\theta_{i,j})$ and $U_{\rm CZ}^{(i)}=\prod_{j=1}^{n-1}{\rm CZ}_{j,j+1},$ where $P_i\in\{X,Y,Z\},$ and $\theta_{i,j}\in[0,2\pi).$

The objective is a single Pauli ZZ operator on the first and second qubits, $\hat{\sigma}_z \otimes \hat{\sigma}_z$. The circuit is visualized in Figure 4. The hyperparameter settings follow Stokes et al. [68] when possible. The default settings are organized in Appendix B. In this experiment, L2O- g^{\dagger} is trained on a single PQC with the configuration of $(N_q, l) = (7, 5)$. By controlling the number of qubits N_q and layers l, we can demonstrate L2O- g^{\dagger} robustness against different numbers of optimization dimensions beyond its training PQC.

b. Results. We summarize our results for optimizing Random PQC in Figure 5 with various qubits N_q and layers l. L2O- g^{\dagger} demonstrates robustness against entirely different random circuits and varying numbers of parameters compared to its training instances. With only one random PQC in its training stage, this highlights L2O- g^{\dagger}

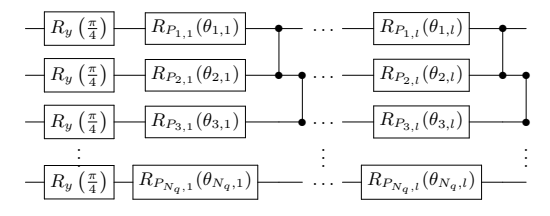


FIG. 4: Illustration of Random Parameterized Quantum Circuit.

ability to generalize optimization strategy.

B. Variational Quantum Eigensolver (VQE)

a. Backgrounds. Variational quantum eigensolver (VQE) was originally proposed by Peruzzo et al. [52] and has become an important algorithm in the VQAs family. It is based on the variational principle of quantum mechanics:

$$E_0 \le \langle \psi | \hat{H} | \psi \rangle. \tag{17}$$

Given a trial wavefunction and Hamiltonian \hat{H} that encodes the problem, VQE finds the ground state energy of the system E_0 with optimal parameters θ^* :

$$\lambda_{\min} = E_0 \approx \langle \psi(\boldsymbol{\theta}^*) | \hat{H} | \psi(\boldsymbol{\theta}^*) \rangle. \tag{18}$$

The Hamiltonian in the second quantization form for a many-body system can be written in terms of the creation operator c^{\dagger} and annihilation operator c:

$$\hat{\boldsymbol{H}} = \sum_{p,q} h_{pq} \boldsymbol{c}_p^{\dagger} \boldsymbol{c}_q + \frac{1}{2} \sum_{p,q,r,s} h_{pqrs} \boldsymbol{c}_p^{\dagger} \boldsymbol{c}_q^{\dagger} \boldsymbol{c}_r \boldsymbol{c}_s.$$
 (19)

b. Ansatz. The simplest ansatz selection is hardware-efficient ansatz (HEA) which is a parameterized quantum circuit tailored to quantum devices [32, 35, 51, 69]. It works flexibly but it needs to span a large Hilbert space so at worst it scales exponentially in the worst case. HEA can be represented in the following form

$$\prod_{l=1}^{L} \left(\prod_{i=1}^{n} U(\theta_{i,l}) \prod_{(i,j) \in E} \text{CNOT}_{ij} \right)$$
 (20)

where n is the number of qubits, L is the number of layers of gates, $U(\theta_{i,l})$ represents a parameterized single-qubit gate on the i-th qubit in the l-th layer, and E represents the set of qubit pairs (i,j) connected by CNOT gates within the hardware's connectivity graph.

The second and third type of ansatz proposed by Barkoutsos et al. [9] are the $U_{\rm ent}^{(1)}$ ansatz and Unitary Coupled-Cluster Singles and Doubles (UCCSD) ansatz. $U_{\rm ent}^{(1)}$ adjust HEA with the constraint of preserving a constant number of particles in the following form proposed by [6, 9]

$$|\Psi(\boldsymbol{\theta})\rangle = U_D(\boldsymbol{\theta})U_{\text{ex}}\dots U_1(\boldsymbol{\theta})U_{\text{ex}}U_0(\boldsymbol{\theta})|\Phi_0\rangle$$
 (21)

where it consist of single-qubit rotations $U_i(\theta)$ at i layers and entagling drift operation $U_{\rm ex}$. In particular $U_{\rm ex}$ can be particle conserving two-parameter exchange-type gate [9] with the following form in Equation (22).

$$U_{\rm ex}(\theta_1, \theta_2) = \begin{pmatrix} 1 & 0 & 0 & 0\\ 0 & \cos \theta_1 & e^{i\theta_2} \sin \theta_1 & 0\\ 0 & e^{-i\theta_2} \sin \theta_1 & -\cos \theta_1 & 0\\ 0 & 0 & 0 & 1 \end{pmatrix}$$
(22)

The third type of ansatz we implement in our experiments is the Unitary Coupled-Cluster Singles and Doubles (UCCSD) ansatz [9]. The Coupled Cluster (CC) ansatz uses these excitations to create a wave function from the Hartree-Fock state as $\Psi = e^{\tilde{T}}\Phi_{\rm HF}$.

$$e^{T-T^{\dagger}}$$
 where $T = T_1 + T_2$ (23)

$$T_1 = \sum_{i,a} t_i^a \boldsymbol{a}_a^{\dagger} \boldsymbol{a}_i, \quad T_2 = \sum_{i,j,a,b} t_{ij}^{ab} \boldsymbol{a}_a^{\dagger} \boldsymbol{a}_b^{\dagger} \boldsymbol{a}_i \boldsymbol{a}_j$$
 (24)

 T_1 represents single excitations, with t_i^a denoting the amplitude for exciting an electron from the occupied spinorbital i to the virtual spin-orbital a. T_2 represents double excitations, with t_{ij}^{ab} as the amplitude for exciting electrons from the occupied orbitals i and j to the virtual orbitals a and b. Here, a_i^{\dagger} and a_i are fermionic creation and annihilation operators, respectively.

c. Setup. We implement three ansatz: HEA, $U_{\rm ent}^{(1)}$, and UCCSD. For HEA, we show that by training L2O- g^{\dagger} on a single bond length of H₂, it can generalize to different bond lengths with relatively small errors. For $U_{\rm ent}^{(1)}$ ansatz, we choose LiH, BeH₂, and H₂O molecules and calculate the ground state energy with various repeated entangle blocks in the ansatz, ranging from D=1 to D=30 entangle blocks. For UCCSD ansatz, we choose H₂, H₃⁺, and H₄ molecules and calculate the approximate ground state energy for various inter-atomic radii. We report the mean of ten runs and the 90% confidence interval, along with two baseline optimizers: RMSprop and Adam.

All the optimizations for various ansatz are taken from randomly initialized parameters and the objective values after 200 iterations. We use randomly initialized parameters for the HEA and UCCSD ansatz and initialize with the Hartree-Fock state for the $U_{\rm ent}^{(1)}$ ansatz. The molecular data are provided by Pennylane datasets [8].

d. Results. We illustrate our results on HEA, $U_{\rm ent}^{(1)}$ ansatz, and UCCSD ansatz in Figure 6, Figure 7, and Figure 8, respectively. For HEA, shown in Figure 6, we demonstrate our method's ability by training on a single instance of the $\rm H_2$ molecule to generalize to solve the ground state energy across various radii. It surpasses other optimization algorithms in terms of convergence speed. For the $U_{\rm ent}^{(1)}$ ansatz, we show its performance by training on a random generic PQC in Section IV A. It achieves near chemical accuracy on most inter-atomic

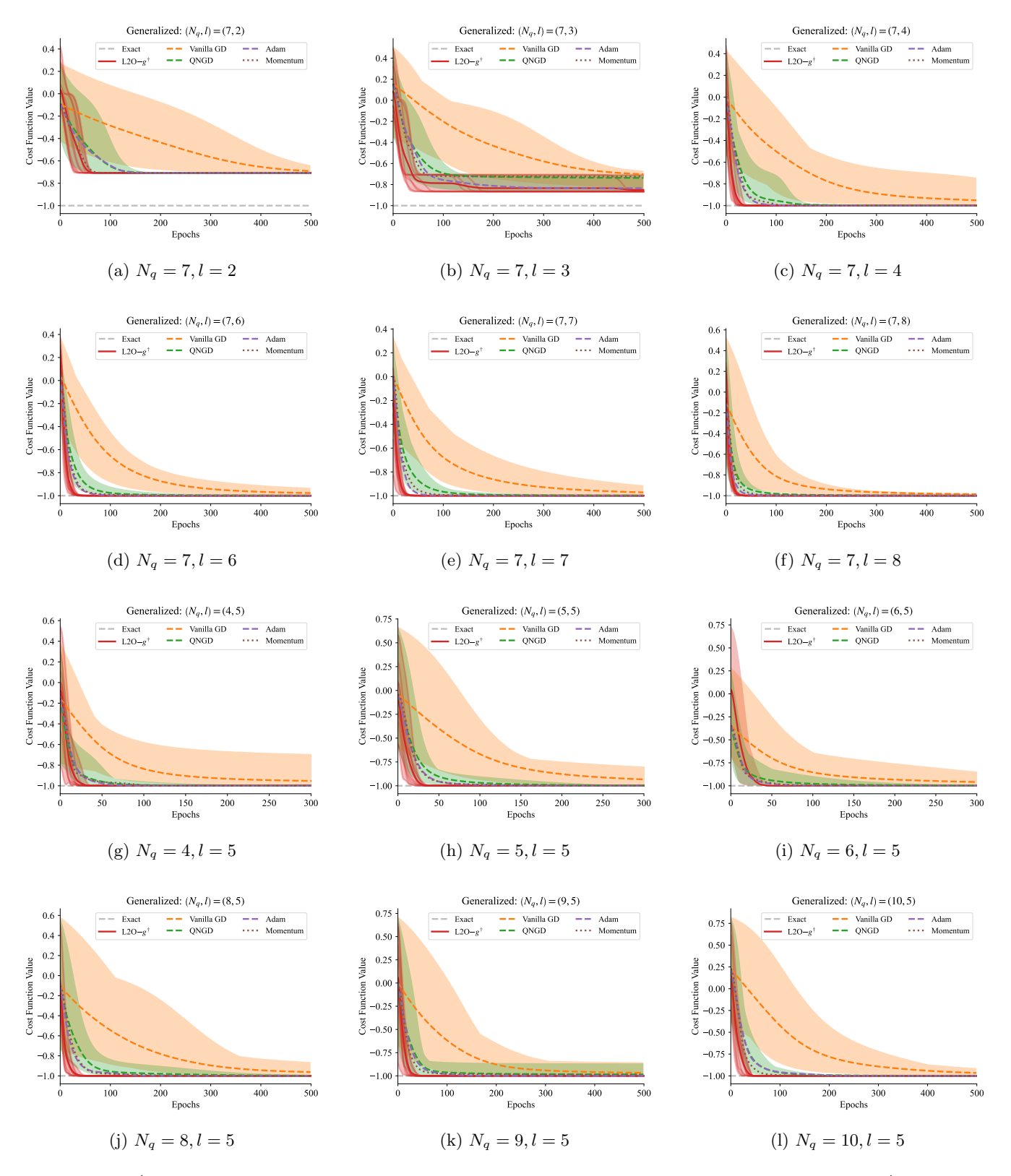


FIG. 5: **L2O**- g^{\dagger} Generalized to Different Random PQC. The upper two rows from (a) to (f) show L2O- g^{\dagger} abilities to adapt to different numbers of layers l from 2 to 8 with $N_q = 7$. In the case of l = 2 and l = 3, all methods do not converge to the optimal value of -1 due to a lack of tunable parameters. However, L2O- g^{\dagger} still reaches the minimum value faster than other baseline optimizers. The bottom two rows from (g) to (l) show L2O- g^{\dagger} abilities to adapt to different numbers of qubits N_q from 4 to 10 with l = 5. L2O- g^{\dagger} consistently outperforms in convergence speed on all configurations and is less sensitive to the initial parameter. In all experiments, we average over 10 different sequences of single qubit gates and plot the average (full color) and each loss curve (lighter color), along with the baseline average (solid line) and standard deviation (ribbon).

radii for more complex molecules like LiH, BeH₂, and $\rm H_2O$ with up to 30 entangled blocks. For the UCCSD ansatz, using the same trained model on the random PQC in Section IV A, our method achieves higher accuracy compared to RMSprop and Adam optimizers. It also shows more robustness against initial parameters, as evidenced by the much smaller 90% confidence intervals for $\rm H_2$, $\rm H_3^+$, and $\rm H_4$ molecules.

C. QAOA for MaxCut

a. Backgrounds. Given an undirected graph $\mathcal{G} = (\mathcal{V}, \mathcal{E})$, where V is the set of vertices, E is the set of edges, and w_{ij} is the weight corresponding to the edge $(i, j) \in E$. The objective of the MaxCut is to partition the graph vertices x_i , for $i = 1, \ldots, |V|$ into two sets where the cost function is defined as

$$C(x) = \sum_{i=1}^{|V|} \sum_{j=1}^{|V|} w_{ij} x_i (1 - x_j).$$
 (25)

MaxCut is NP-hard, meaning no poly-time algorithm solves for all instances assuming P \neq NP (NP-Completeness). Therefore, we rely on approximate solutions. We can define the approximation ratio α for an objective function \mathcal{C} as

$$\alpha = \frac{\mathcal{C}(\boldsymbol{x}^*)}{\mathcal{C}_{\text{max}}} \tag{26}$$

where $C(x^*)$ is the value of the objective function for the approximate solution x^* , and \mathcal{C}_{max} is the value of the objective function for the optimal solution. The bestperforming classical approximation algorithm for the MaxCut problem is the Goemans-Williamson algorithm, which achieves an approximation ratio of $\alpha \approx 0.878$. QAOA was first proposed by Farhi et al. [22]. It consists of a parameterized quantum circuit with layer p_{layer} , where each layer includes cost layers $\hat{U}_C(\gamma_p)$ and mixer layers $\hat{U}_M(\beta_p)$. QAOA maps the cost function \mathcal{C} into the Hamiltonian of the circuit. It uses variational parameters (γ, β) , which are the cost layer and mixer layer parameters, respectively. In total, there are $2p_{\text{layer}}$ parameters in a QAOA problem. Regarding the potential of QAOA for the MaxCut problem, Farhi et al. [22] show that for the 3-regular graph MaxCut problem, QAOA achieves a worst-case $\alpha \geq 0.6924$ for $p_{\text{layer}} = 1$.

b. Setup. We construct our map with randomly generated Erdős-Rényi graph $\mathcal{G}(V,p)$ (see Figure 13). Each pair of V vertices is connected by an edge given with probability p. The ER graph for different V and p is illustrated in Figure 9. We select the ER graph since we can control the difficulty and characteristics of the problem with parameters V and p. We implement the baseline quantum natural gradient descent (QNGD) [68] with a log-uniform learning rate between 10^{-2} to 10^{-4} and each learning rate is averaged over five random initial parameters. For L2O- g^{\dagger} , we only average over the

same five random initial parameters since it does not have any hyperparameters and report the mean and standard deviation. We train L2O- g^{\dagger} on the simplest graph (V,p)=(5,0.5) mark in blue in Figure 9. We set the repeated layer $p_{\rm layer}=3$ for all graphs.

c. Results. Figure 9 shows the results for the Max-Cut problem on the ER graph with $p \in [0.5, 0.6, 0.7]$ and $V \in [5, 6, 7]$. Incidentally, the ER graph coincides for V = 5 at p = 0.6 and p = 0.7. By training L2O- g^{\dagger} on a simple ER graph, we show that it can match or surpass learning rate-tuned quantum natural gradient descent on various levels of graph complexity. In the cases where L2O- g^{\dagger} achieves similar results with QNGD, we identify the possible reason for being sensitive to initial parameters.

D. QAOA for Sherrington-Kirkpatrick Model

a. Backgrounds. Extending the QAOA method from the MaxCut problem in Section IV C, in this section we apply QAOA to the Sherrington-Kirkpatrick model. The SK model [65] is a mean-field model for an all-to-all coupling spin glass. Consider n Ising spins given by

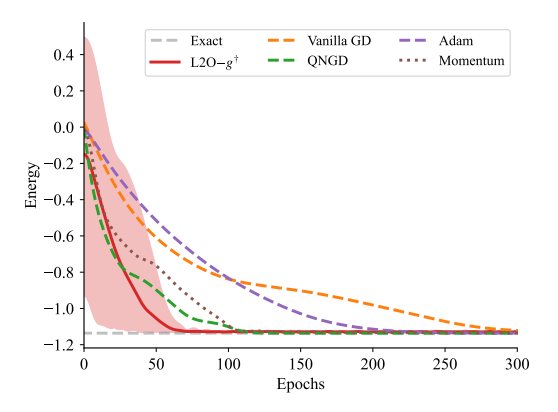
$$\sigma = (z_1, \dots, z_n) \in \{-1, +1\}^n \tag{27}$$

The cost function is defined as

$$C = \frac{1}{\sqrt{n}} \sum_{i < j} J_{ij} z_i z_j \tag{28}$$

where $J_{ij}=\pm 1$ in our experiment. Regarding the potential of QAOA for the SK model, Farhi et al. [23] demonstrates that the QAOA achieves a higher approximation ratio at p=11 than the classical Semi-Definite Programming (SDP) method. QAOA showcases the potential for solving the SK model better than the classical SDP method. Generally, the more layers of the QAOA the more expressibility the circuit becomes, therefore it can achieve lower objective values (cost function).

- b. Setup. We test L2O- g^{\dagger} on an n=8 SK model, trained on the same ER graph as Section IV C with the configuration of (V,p)=(5,0.5). We select a wide variety of hand-designed optimizers and evaluate them on default hyperparameters (Appendix B), including RM-Sprop, Adam, GD, QNGD, Momentum, and Adagrad. We experiment with QAOA layers from $p_{\text{layer}}=1$ to $p_{\text{layer}}=5$ and report the average and standard deviation over five runs of the final objective value after 10 and 200 iterations.
- c. Results. In Figure 10, L2O- g^{\dagger} showcase generalizability and performance by applying QAOA to the SK model after training on a general MaxCut problem of a random ER graph. L2O- g^{\dagger} match or surpass hand-designed optimizers without tuning any hyperparameters and converge faster, as evidenced by the final objective value after 10 iterations (lighter color in Figure 10).



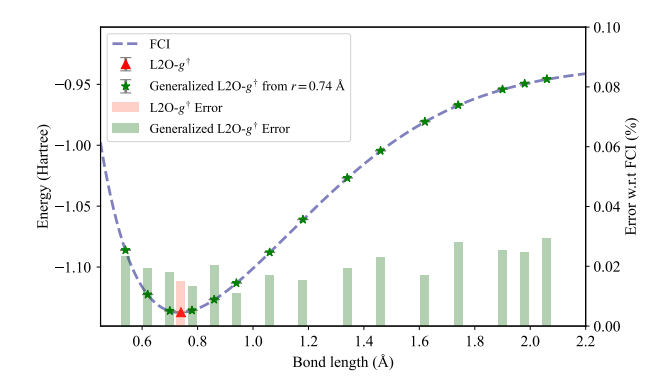


FIG. 6: (Left) Applying VQE for H₂ using L2O- g^{\dagger} . We experiment with ten different initial parameters and report the average (line) and standard deviation (ribbon). L2O- g^{\dagger} converges faster than other baseline optimizers for solving the ground state energy of H₂. The grey line is calculated by the FCI model for the exact ground state energy of H₂ at the inter-atomic equilibrium distance r = 0.7 Å. (Right) L2O- g^{\dagger} ability to Generalize on Various Bond Lengths of Optimizing VQE for H₂. L2O- g^{\dagger} is trained on a single instance from r = 0.74Å (mark in red) and then uses the model to optimize various inter-atomic radii (mark in green). We report the average as well as the standard deviation after 200 iterations of 10 runs and report the relative error to the FCI energy in percentages.

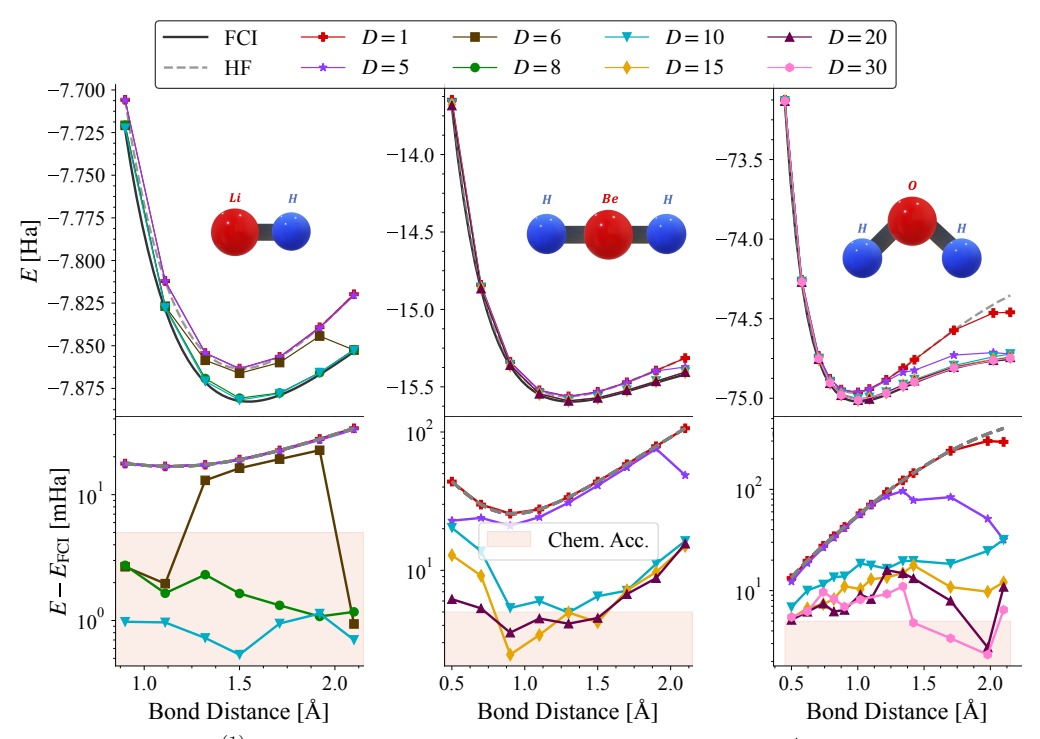


FIG. 7: Applying VQE with $U_{\rm ent}^{(1)}$ Ansatz for LiH, BeH₂, and H₂O using L2O- g^{\dagger} Trained on Random PQC. For every bond length, we report the average over three random seeds and plot the dissociation profile of various molecules, including LiH, BeH₂, and H₂O, at different numbers of repeated entangle blocks. As expected, in the lower panel, as we increase the number of entangle blocks, the difference between VQE results and FCI decreases and is even smaller than chemical accuracy in many cases. The chemical accuracy is set to 0.5×10^{-2} Ha following Barkoutsos et al. [9]. L2O- g^{\dagger} is robust against increasing layers and is even capable of optimizing up to D = 30.

E. Data Re-upload Classifier

a. Backgrounds. A quantum neural network consists of three major parts: data encoding, state evolution, and measurement. First, data encoding takes the input data $x \in \mathbb{R}^{x_{dim}}$ and maps it into an N_q qubits Hilbert

space with the feature map $|\psi_x\rangle = U_{enc}|0\rangle^{\otimes N_q}$. Second, the state evolves with variational unitary $|\psi_{\theta}(x)\rangle = U_{\theta}|\psi_x\rangle$. Finally, perform measurement on N_q qubits. Combining these steps into a single equation, we get:

$$|\psi_{\theta}(x)\rangle = U_{\theta}U_{enc}|0\rangle^{\otimes N_q}.$$
 (29)

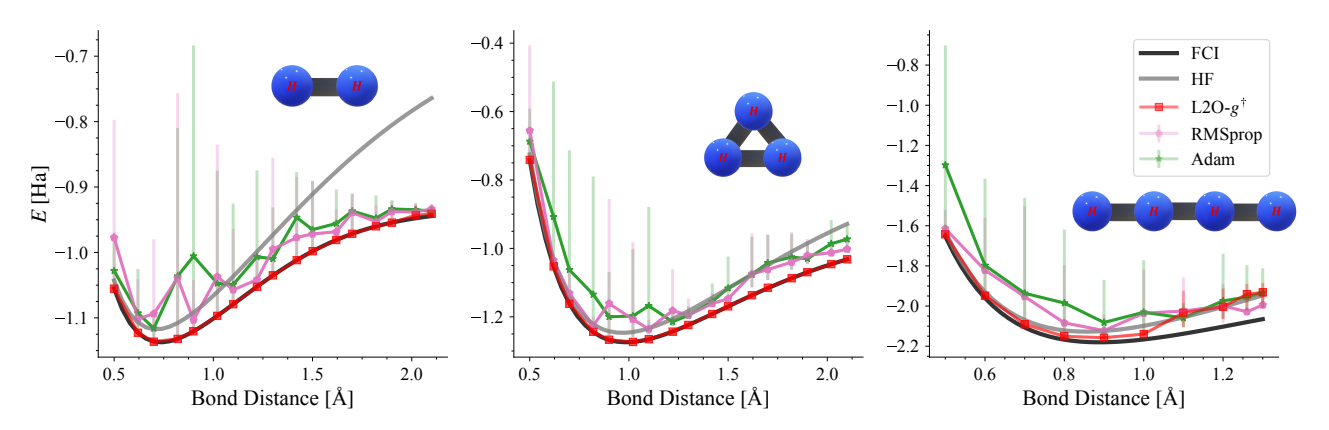


FIG. 8: Applying VQE with UCCSD Ansatz for H_2 , H_3^+ , H_4 using L2O- g^{\dagger} Trained on Random PQC. We report the 90% confidence interval for every bond length along with FCI energy and HF energy. The confidence intervals for H_2 and H_3^+ of L2O- g^{\dagger} are too small to be visible.

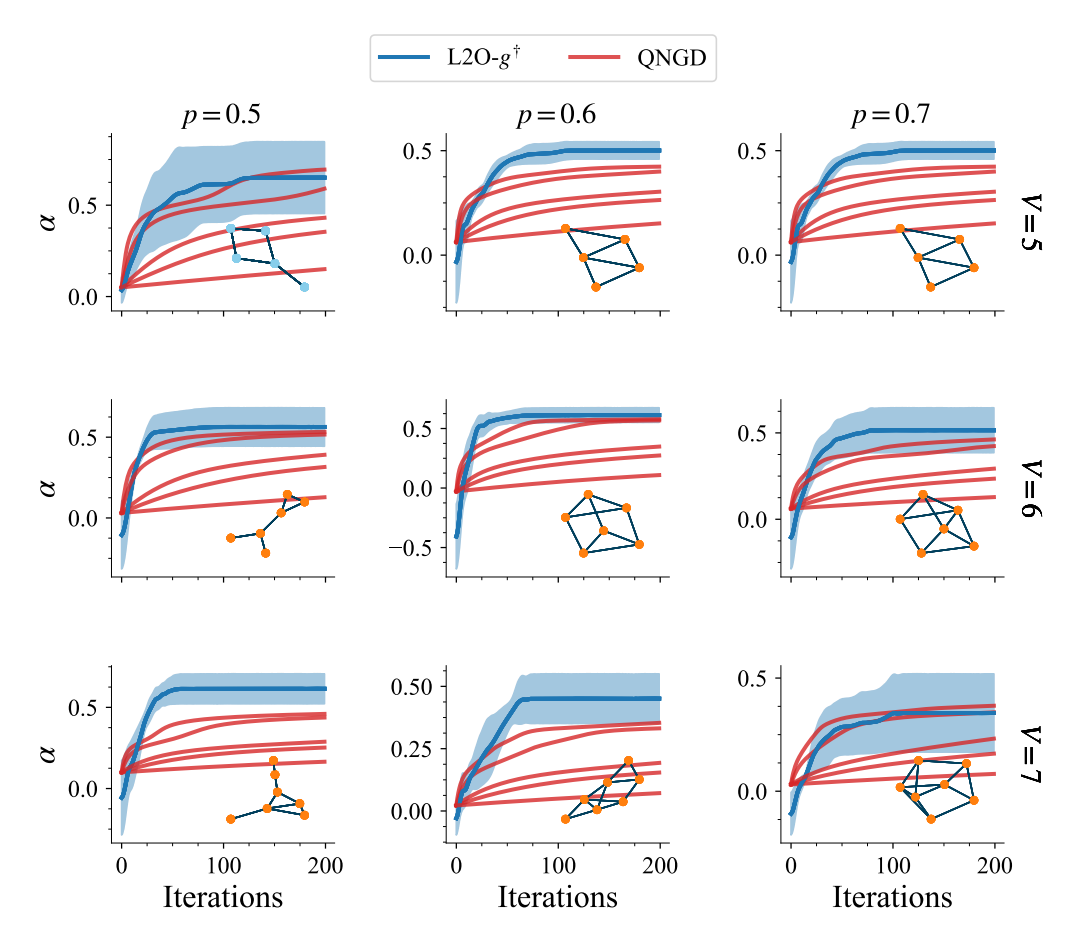


FIG. 9: Approximation Ratio for the Maxcut Problem with $p_{\text{layer}} = 3$ for Randomly Generating the Erdős-Rényi Graph. We train L2O- g^{\dagger} on the simplest graph (V, p) = (5, 0.5) mark in blue. We run the QNGD with five different learning rates, ranging logarithmically from 10^{-2} to 10^{-4} , and averaged the results over five random initial parameters. L2O- g^{\dagger} match or surpass QNGD with the best hyperparameter configuration on every graph. We report the results of L2O- g^{\dagger} over the same five random initial parameters and plot the standard deviation in the ribbon. In the cases where QNGD matches L2O- g^{\dagger} happens when the standard deviation is larger, which may be attributed to increased sensitivity to the initial parameters.

Quantum neural network is the study of data and information with a quantum circuit (see [11, 13, 62] for

more detail). Abbas et al. [2] show that quantum neural networks have favorable training landscapes and achieve

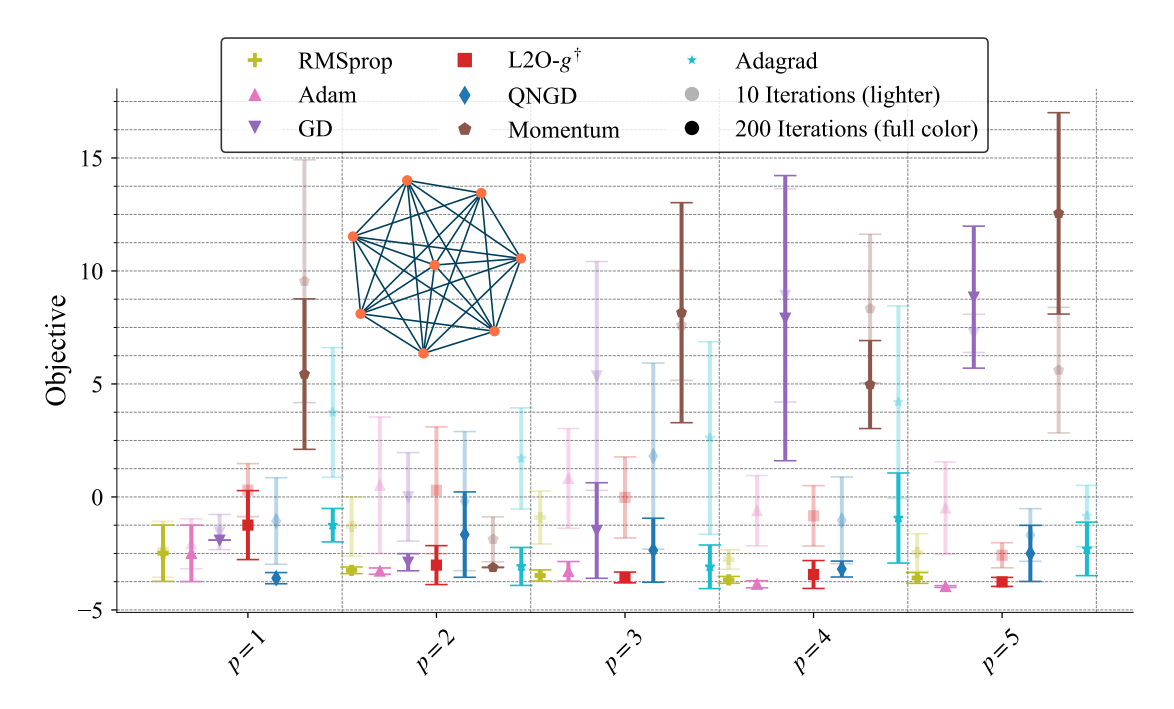


FIG. 10: Applying QAOA for Sherrington-Kirkpatrick Model with n=8 and $p_{\rm layer} \in [1,5]$. We plot the final objective values after 10 iterations (lighter color) and after 200 iterations (full color) of various optimizers, including RMSprop, Adam, GD, QNGD, Momentum, and Adagrad, with default hyperparameters. All experiments are repeated five times for every configuration, and we report the mean and standard deviation. L2O- g^{\dagger} consistently converge to lower objective values with relatively small standard deviations, especially converging faster as evidenced by the objective values after ten iterations.

higher effective dimensions compared to classical neural nets. The data re-upload classifier is one of them. Data re-upload classifier was proposed by Pérez-Salinas et al. [57]. They theoretically and experimentally prove that a single qubit is sufficient to construct a universal quantum classifier. Here we summarize the data-reupload classifier following Bowles et al. [13]. Classical neural networks process original data several times for each neuron in the first hidden layers. On the other hand, the re-upload classifier uses successive, trainable angle embeddings of data. For a vector \boldsymbol{x} of three features, two trainable three-dimensional real vectors \boldsymbol{w} and $\boldsymbol{\theta}$, and encodes them as

$$U(\boldsymbol{x} \circ \boldsymbol{\omega} + \boldsymbol{\theta}) \tag{30}$$

where

$$U(\phi) = e^{iZ\phi_1/2}e^{iY\phi_2/2}e^{iZ\phi_3/2}.$$
 (31)

To encode a data $\mathbf{x} \in \mathbb{R}^d$, we split x into [d/3] vector. The fidelity cost function is based on the output qubits to one of the states $|0\rangle$, $|1\rangle$. $F_{0_j}(\mathbf{x})$, $F_{1_j}(\mathbf{x})$ is the fidelity of the j-th qubit. The cost function is defined as

$$C(\theta, \omega, \alpha, \mathbf{x}_i) = \sum_{j=1}^{n_{\text{max}}} (\alpha_{0_j} F_{0_j} - (1 - y_i))^2 + (\alpha_{1_j} F_{1_j} - y_i)^2$$
(32)

where α_{0_j} , α_{1_j} are trainable parameters. When predicting, we use average fidelity either $|0\rangle$ or $|1\rangle$ over the same qubits:

$$y_{\text{pred}} = \arg\max(\langle F_{0_i} \rangle, \langle F_{1_i} \rangle). \tag{33}$$

b. Setup. We test L2O- g^{\dagger} on data re-upload classifier, trained with random PQC from Section IVA. Experiments were conducted using a single qubit classifier across multiple layers $l \in \{1, 3, 5, 8, 10\}$. Baseline results are quoted from Pérez-Salinas et al. [57] when available, and reproduced otherwise. Following the experimental setup in Pérez-Salinas et al. [57]. We use a data reupload classifier to determine whether points lie inside or outside a circle. It classifies points within a circular boundary defined by $\mathbf{x} = (x_1, x_2)$, where $x_i \in [-1, 1]$ and $x_1^2 + x_2^2 < r^2$. The radius r is set to $\sqrt{2}$. We generated a training dataset with 200 datapoints and a testing dataset with 4000 datapoints. We then average the results three times to evaluate the model's performance. We further conducted 20 random learning rate searches between 10^{-2} and 10^{-4} for Adam and Momentum and compare them with a single trial L2O- g^{\dagger} .

c. Results. We summarize the results in Figure 11 and Table I. In Figure 11 (Left), we show that replacing the second-order optimizer L-BFGS-B used in Pérez-Salinas et al. [57] with L2O- g^{\dagger} boosts the performance of the data re-upload classifier. The final accuracy for L2O- g^{\dagger} , L-BFGS-B, gradient descent, Adam, and Momentum

are summarized in Table I. In Figure 11 (Right), L2O- g^{\dagger} uniformly matches or outperforms 20 random learning rate search Adam optimizer and Momentum optimizer with a single trial L2O- g^{\dagger} optimizer. L2O- g^{\dagger} learns a good optimization strategy with minimum effort and showcases convincing results both in terms of optimization wall time and consistency of convergence speed. This brings QNNs a step closer to classical neural networks, as evidenced in the case of l=10. These results highlight that the selection of the optimizer is as crucial as the neural network architecture itself. By training on a generic PQC, L2O- g^{\dagger} can tackle drastically different tasks.

LAYERS	1	3	5	8	10
	50*			93*	95*
Vanilla GD	44.47	49.40	48.41	43.34	47.58
	56.14				
Adam	50.31	79.58	84.33	83.88	86.08
$\mathbf{L2O}$ - g^{\dagger}	50.25	90.88	91.37	95.34	95.50
C. NN			96*		
C. SVC			97^*		

TABLE I: Accuracy on Various Layers in Data Re-Upload Classifier. We report the average accuracy over three runs. L2O- g^{\dagger} achieve near optimal score for all layers in data re-upload classifier, even surpassing second-order optimizer L-BFGS-B. Results quoted from Pérez-Salinas et al. [57] are marked with *. When unavailable, we reproduce optimizer results independently.

F. Ablation Studies

We conduct the following ablation studies on L2O- g^{\dagger} :

a. Compare with LSTM Learned Optimizer. In Table II, we compare L2O- g^{\dagger} with L2O-DM [4], which has been used with the same architecture in Verdon et al. [71], Wilson et al. [73], utilizing a simple coordinate-wise LSTM. Both models are trained on a single random PQC with the configuration of $(N_q, l) = (7, 5)$. We randomly select a range from three to six configurations for every problem detailed in Sections IV A to IV E and report the average and standard deviation of either loss, approximation ratio, or accuracy over five runs. The results show that L2O- g^{\dagger} significantly improves its performance and generalizability from previously learned optimizer despite only being trained on a single generic PQC instance.

b. Curriculum Learning. In Figure 12, we train a separate model without curriculum learning as detailed in Section III. Without curriculum learning, the test loss is significantly higher while the training loss is roughly of the same magnitude as the model using curriculum learning. The results highlight that curriculum learning can improve generalizability and provide a more stable training process. Specifically, $L2O-g^{\dagger}$ only takes roughly 100 trajectories to reach a stable minimum and is able

to generalize well on totally different problems (see Table II).

V. RELATED WORKS

In this section, we organize related work for deep learning and quantum computing Section VA, learned optimizer for neural networks Section VB and learned optimizer for PQC Section VC.

A. Deep Learning and Quantum Computing

Rapid developments in deep learning and quantum computing have drastically widened our imagination about future applications and computing. Deep learning is a machine learning model that fits the domains of data [56]. It has shown extraordinary capacity across various domains, including natural language [3, 70], computer vision [20, 67], time-series forecasting [59, 74, 78, 81], speech recognition [58, 80], tabular learning [25, 76], and reinforcement learning for control systems [75]. In particular, the advent of the transformer-based foundation model in language generation [30, 42, 77], genomics domain [82, 83] and vision transformer [31] has significantly advanced the field, showing impressive performance. Many works combine deep learning with quantum computing in hybrid variational quantum algorithms, including learned optimizers [71, 73] and quantum-classical neural networks [7, 44]. In the next sections, we organize works that apply deep learning models to either classical neural networks Section VB or parameterized quantum circuits Section VC to learn to optimize.

B. Learning to Optimize Neural Networks

The first major development for learned optimizers was proposed by Andrychowicz et al. [4], who showed that a simple coordinate-wise LSTM model can outperform hand-designed models on similar tasks from its training sets. However, it does not generalize well to different neural network architectures far from its training dataset distribution. Training techniques are especially important for meta-learning optimizers since the process of backpropagation through a cumulative rolling length makes it unstable. Metz et al. [48] show that chaotic dynamics may appear when training a learned optimizer. Chen et al. [17] further incorporate additional features such as validation loss and show that by training on large instances, they can generalize well even when training themselves from scratch. Several researchers have identified the importance of training techniques for learned optimizers and empirically show improvements in the variety of SOTA optimizers. For example, Chen et al. [17] use curriculum learning and imitation learning to

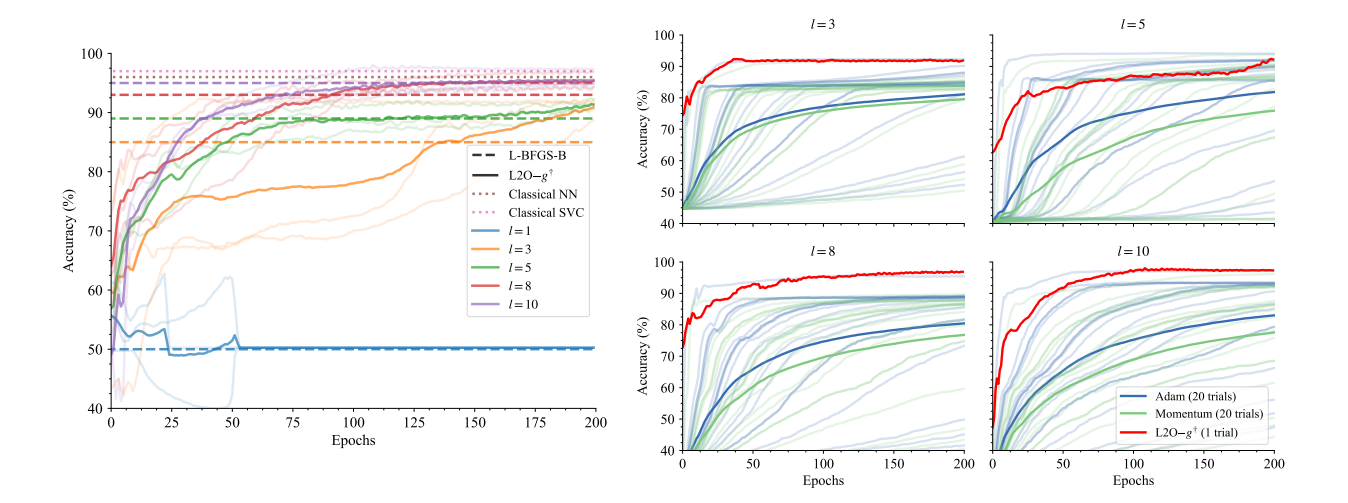


FIG. 11: (Left) Accuracy of L2O- g^{\dagger} on Optimizing Re-upload Circuit on Circular Boundary Classification Problem with $l \in \{1, 3, 5, 8, 10\}$. The results are averaged over three runs and shown in solid-colored lines. The lighter color corresponds to each of the three runs for every configuration. Horizontal dashed lines are quoted from Pérez-Salinas et al. [57] using the L-BFGS-B optimizer, a second-order optimizer. The horizontal dotted lines are also quoted from Pérez-Salinas et al. [57] for classical neural network results. L2O- g^{\dagger} surpasses the L-BFGS-B optimizer by reaching higher accuracy after a few iterations. (Right) Compare the Performance of a Single Trial L2O- g^{\dagger} with 20 Random Learning Rate Search Adam and Momentum Optimizer. We average over three runs for every configuration with the same training sets and initial parameters. L2O- g^{\dagger} match or surpass 20 random learning rate tuned Adam and Momentum optimizer.

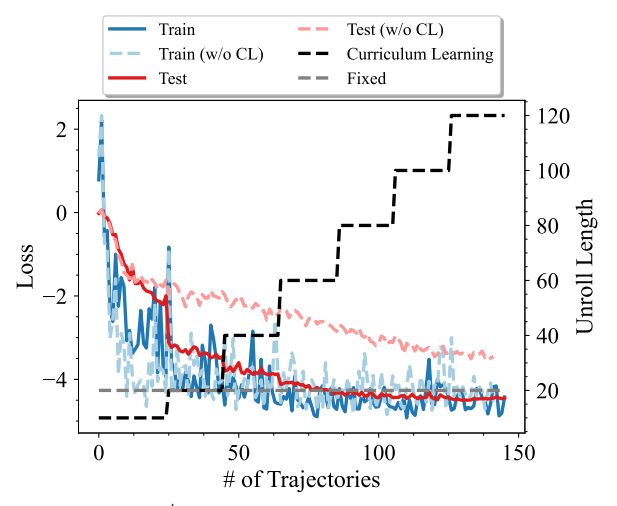


FIG. 12: L2O- g^{\dagger} Training and Testing Loss with or without Curriculum Learning. The training loss exhibits a similar trend with or without curriculum learning. However, the testing loss for L2O- g^{\dagger} is significantly lower and converges faster than without curriculum learning. The black and grey dashed lines correspond to unroll length after the number of trajectories. The y-axis corresponds to the number of trajectories trained by the model.

improve training stability and generalizability; Verdon et al. [71] propose random scaling and incorporate convex functions to improve the generalizability of learned optimizers. Instead of using a black-box model, Chen et al. [18] use symbolic learning to discover new optimization

algorithms. Metz et al. [50] scale up the training sets for the learned optimizer and use extensive training on a wide variety of deep learning problems, showing that the learned optimizer demonstrates superior performance in terms of time saved for hyperparameter optimization.

C. Learning to Optimize Parameterized Quantum Circuits

Verdon et al. [71], Wilson et al. [73] utilized same architecture as Andrychowicz et al. [4]. However, it can only serve as an initializer and is limited to similar optimization tasks in their training sets. Another work by Kulshrestha et al. [38] also uses a similar architecture to Andrychowicz et al. [4], they use the change in the cost function to approximate the gradient as the input feature. Their tasks are limited to a fixed PQC for quantum machine learning tasks. Other lines of work by Lockwood [41] utilizing Reinforcement Learning (RL) to augment gradient descent algorithm. Their results show that the performance critically depends on the structure of the ansatz. Previous studies on learned optimizers for PQC demonstrate their ability to optimize VQAs in limited scenarios outside the training distribution.

PROBLEM	Config.	L2O-DM [4]	${f L2O} ext{-}g^{\dagger}$ (ours)
Rand. $PQC(\downarrow)$		-1.00 ± 0.00 -0.94 ± 0.06 -1.00 ± 0.00	$\begin{array}{c} \textbf{-1.00} \pm 0.00 \\ \textbf{-1.00} \pm 0.00 \\ \textbf{-1.00} \pm 0.00 \end{array}$
${\text{VQE/HEA}(\downarrow)}$	$egin{array}{ c c c c } H_2 & \text{AT } r = 0.5 \\ H_2 & \text{AT } r = 0.9 \\ H_2 & \text{AT } r = 1.5 \\ \hline \end{array}$	$\begin{array}{l} -0.27 \pm 0.31 \\ -0.52 \pm 0.11 \\ -0.56 \pm 0.06 \end{array}$	$\begin{array}{l} \textbf{-0.66} \pm 0.48 \\ \textbf{-0.86} \pm 0.21 \\ \textbf{-0.93} \pm 0.05 \end{array}$
$\mathbf{VQE}/\mathbf{ENT}(\downarrow)$		-7.61 ± 0.03 -15.23 ± 0.03 -74.85 ± 0.01	$\begin{array}{l} \textbf{-7.71} \pm 0.00 \\ \textbf{-15.34} \pm 0.00 \\ \textbf{-74.95} \pm 0.00 \end{array}$
$\mathbf{VQE}/\mathbf{UCCSD}(\downarrow)$	H_2 at $r = 0.5$ H_2 at $r = 0.9$ H_3^+ at $r = 0.5$ H_4^+ at $r = 0.9$ H_4 at $r = 0.5$ H_4 at $r = 0.9$	$\begin{array}{c} -0.87 \pm 0.20 \\ -1.07 \pm 0.06 \\ -0.53 \pm 0.19 \\ -0.79 \pm 0.31 \\ -0.15 \pm 0.60 \\ -1.24 \pm 0.21 \end{array}$	$egin{array}{l} -1.06 \pm 0.00 \ -1.12 \pm 0.00 \ -0.74 \pm 0.00 \ -1.27 \pm 0.00 \ -1.47 \pm 0.35 \ -2.07 \pm 0.17 \end{array}$
$\mathbf{MaxCut}(\uparrow)$		34.78 ± 12.32 49.06 ± 9.66 28.67 ± 9.95	$\begin{matrix} 56.36 \pm 11.90 \\ 61.56 \pm 6.36 \\ 51.53 \pm 12.97 \end{matrix}$
SK $Model(\downarrow)$	$egin{array}{ l l l l l l l l l l l l l l l l l l l$	-0.93 ± 0.95 -1.95 ± 1.65 -1.95 ± 2.12	-0.90 ± 1.10 -2.96 ± 0.06 -2.96 ± 0.05
Data Re-upload(↑	$\begin{vmatrix} l = 3 \\ l = 5 \\ l = 8 \end{vmatrix}$	66.87 ± 1.60 69.50 ± 7.80 81.97 ± 3.60	$\begin{array}{c} 90.08 \pm 1.57 \\ 91.36 \pm 0.70 \\ 95.34 \pm 1.09 \end{array}$

TABLE II: Ablation Study on L2O-DM [4] for Different Problems and Configurations. We report the average and standard deviation of final values after 200 iterations over five runs. The pink column highlights the configurations we train on L2O-DM [4] as well as L2O- g^{\dagger} . For Random PQC, VQE/HEA, VQE/UCCSD, VQE/ENT, and the SK Model we report the final loss. For the MaxCut problem, we report the final approximation ratio. For the Data Re-upload problem, we report the final accuracy. An arrow pointing downward (\downarrow) indicates that lower values are better, while an arrow pointing upward (\uparrow) indicates that higher values are better. L2O- g^{\dagger} show significantly better generalization away from their training task by converging to lower values.

VI. CONCLUSION

In this paper, we present L2O- g^{\dagger} , a quantum-aware learned optimizer that can generalize to a wide variety of parameterized quantum circuits by leveraging parameter space and distribution space optimization. L2O- g^{\dagger} is tailored for optimizing parameterized quantum circuits, requiring minimal training instances, and experimentally shows strong out-of-distribution generalization with the ability to optimize diverse VQAs like VQE, QAOA, and QNN. Importantly, we demonstrate that out-of-the-box L2O- g^{\dagger} can match or surpass learning rate-tuned optimizers like Adam and QNGD, as well as previous work on learned optimizers for PQC, in terms of generalization and convergence speed.

However, implementing VQAs on a large scale in the NISQ era poses additional challenges for surpassing classical computers. These challenges include trainability, efficiency, error mitigation, and scaling up VQAs. Our work takes a small step toward addressing the intrinsic hard problems of optimizing VQAs.

VII. LIMITATIONS

The current learned optimizer architecture is quite simplistic. Incorporating more advanced deep learning models [14, 49, 50] and training techniques [48, 72] into the quantum-aware learned optimizer are crucial future directions. While we strive to benchmark a wide variety of cases on L2O- g^{\dagger} to test the out-of-distribution performance from training on a single PQC instance, there may still be instances where the learned optimizer struggles. Additionally, an important direction for future work is to scale up the training sets, as highlighted in Metz et al. [50], to thoroughly test the scalability of the learned optimizer.

ACKNOWLEDGMENTS

H.-S.G. acknowledges support from the National Science and Technology Council, Taiwan under Grants No. NSTC 113-2119-M-002 -021, No. NSTC112-2119-M-002-014, No. NSTC 111-2119-M-002-007, and No. NSTC 111-2627-M-002-001, from the US Air Force Office of Scientific Research under Award Number FA2386-20-

1-4052, and from the National Taiwan University under Grants No. NTU-CC-112L893404 and No. NTU-CC-113L891604. H.-S.G. is also grateful for the support from the "Center for Advanced Computing and Imaging in Biomedicine (NTU-113L900702)" through The Featured Areas Research Center Program within the framework of the Higher Education Sprout Project by the Ministry of Education (MOE), Taiwan, and the support from the Physics Division, National Center for Theoretical Sciences, Taiwan.

- [1] Suppressing quantum errors by scaling a surface code logical qubit. *Nature*, 614(7949):676–681, 2023. 1
- [2] Amira Abbas, David Sutter, Christa Zoufal, Aurélien Lucchi, Alessio Figalli, and Stefan Woerner. The power of quantum neural networks. *Nature Computational Sci*ence, 1(6):403–409, 2021. 10
- [3] Josh Achiam, Steven Adler, Sandhini Agarwal, Lama Ahmad, Ilge Akkaya, Florencia Leoni Aleman, Diogo Almeida, Janko Altenschmidt, Sam Altman, Shyamal Anadkat, et al. Gpt-4 technical report. arXiv preprint arXiv:2303.08774, 2023. 12
- [4] Marcin Andrychowicz, Misha Denil, Sergio Gomez, Matthew W Hoffman, David Pfau, Tom Schaul, Brendan Shillingford, and Nando De Freitas. Learning to learn by gradient descent by gradient descent. Advances in neural information processing systems, 29, 2016. 2, 4, 12, 13, 14
- [5] Andrew Arrasmith, Zoë Holmes, Marco Cerezo, and Patrick J Coles. Equivalence of quantum barren plateaus to cost concentration and narrow gorges. *Quantum Sci*ence and Technology, 7(4):045015, 2022. 3
- [6] Juan Miguel Arrazola, Olivia Di Matteo, Nicolás Quesada, Soran Jahangiri, Alain Delgado, and Nathan Killoran. Universal quantum circuits for quantum chemistry. Quantum, 6:742, 2022. 6
- [7] Davis Arthur and Prasanna Date. A hybrid quantumclassical neural network architecture for binary classification, 2022. 12
- [8] Utkarsh Azad. Pennylane quantum chemistry datasets, 2023. 6
- [9] Panagiotis Kl Barkoutsos, Jerome F Gonthier, Igor Sokolov, Nikolaj Moll, Gian Salis, Andreas Fuhrer, Marc Ganzhorn, Daniel J Egger, Matthias Troyer, Antonio Mezzacapo, et al. Quantum algorithms for electronic structure calculations: Particle-hole hamiltonian and optimized wave-function expansions. *Physical Review A*, 98 (2):022322, 2018. 5, 6, 9
- [10] Kishor Bharti, Alba Cervera-Lierta, Thi Ha Kyaw, Tobias Haug, Sumner Alperin-Lea, Abhinav Anand, Matthias Degroote, Hermanni Heimonen, Jakob S. Kottmann, Tim Menke, Wai-Keong Mok, Sukin Sim, Leong-Chuan Kwek, and Alán Aspuru-Guzik. Noisy intermediate-scale quantum algorithms. Reviews of Modern Physics, 94(1), February 2022. ISSN 1539-0756.
- [11] Jacob Biamonte, Peter Wittek, Nicola Pancotti, Patrick Rebentrost, Nathan Wiebe, and Seth Lloyd. Quantum machine learning. *Nature*, 549(7671):195–202, 2017. 5, 10
- [12] Lennart Bittel and Martin Kliesch. Training variational quantum algorithms is np-hard. Phys. Rev. Lett., 127: 120502, Sep 2021. 1, 3
- [13] Joseph Bowles, Shahnawaz Ahmed, and Maria Schuld. Better than classical? the subtle art of benchmarking quantum machine learning models, 2024. 10, 11
- [14] Yue Cao, Tianlong Chen, Zhangyang Wang, and Yang Shen. Learning to optimize in swarms. Advances in neural information processing systems, 32, 2019. 14
- [15] Marco Cerezo, Andrew Arrasmith, Ryan Babbush, Simon C Benjamin, Suguru Endo, Keisuke Fujii, Jarrod R McClean, Kosuke Mitarai, Xiao Yuan, Lukasz Cincio, et al. Variational quantum algorithms. *Nature Reviews Physics*, 3(9):625–644, 2021.

- [16] Marco Cerezo, Akira Sone, Tyler Volkoff, Lukasz Cincio, and Patrick J Coles. Cost function dependent barren plateaus in shallow parametrized quantum circuits. Nature communications, 12(1):1791, 2021. 1
- [17] Tianlong Chen, Weiyi Zhang, Zhou Jingyang, Shiyu Chang, Sijia Liu, Lisa Amini, and Zhangyang Wang. Training stronger baselines for learning to optimize. Advances in Neural Information Processing Systems, 33: 7332–7343, 2020. 4, 12
- [18] Xiangning Chen, Chen Liang, Da Huang, Esteban Real, Kaiyuan Wang, Hieu Pham, Xuanyi Dong, Thang Luong, Cho-Jui Hsieh, Yifeng Lu, et al. Symbolic discovery of optimization algorithms. Advances in Neural Information Processing Systems, 36, 2024. 13
- [19] Andrew J Daley, Immanuel Bloch, Christian Kokail, Stuart Flannigan, Natalie Pearson, Matthias Troyer, and Peter Zoller. Practical quantum advantage in quantum simulation. *Nature*, 607(7920):667–676, 2022. 1
- [20] Alexey Dosovitskiy, Lucas Beyer, Alexander Kolesnikov, Dirk Weissenborn, Xiaohua Zhai, Thomas Unterthiner, Mostafa Dehghani, Matthias Minderer, Georg Heigold, Sylvain Gelly, Jakob Uszkoreit, and Neil Houlsby. An image is worth 16x16 words: Transformers for image recognition at scale, 2021. 12
- [21] John Duchi, Elad Hazan, and Yoram Singer. Adaptive subgradient methods for online learning and stochastic optimization. *Journal of machine learning research*, 12 (7), 2011. 4
- [22] Edward Farhi, Jeffrey Goldstone, and Sam Gutmann. A quantum approximate optimization algorithm, 2014. 1, 5, 8
- [23] Edward Farhi, Jeffrey Goldstone, Sam Gutmann, and Leo Zhou. The quantum approximate optimization algorithm and the sherrington-kirkpatrick model at infinite size. *Quantum*, 6:759, 2022. 8
- [24] Julien Gacon, Christa Zoufal, Giuseppe Carleo, and Stefan Woerner. Simultaneous perturbation stochastic approximation of the quantum fisher information. *Quan*tum, 5:567, October 2021. ISSN 2521-327X. 1
- [25] Yury Gorishniy, Ivan Rubachev, Nikolay Kartashev, Daniil Shlenskii, Akim Kotelnikov, and Artem Babenko. Tabr: Tabular deep learning meets nearest neighbors. In The Twelfth International Conference on Learning Representations, 2024. 12
- [26] Edward Grant, Leonard Wossnig, Mateusz Ostaszewski, and Marcello Benedetti. An initialization strategy for addressing barren plateaus in parametrized quantum circuits. Quantum, 3:214, December 2019. ISSN 2521-327X.
- [27] Harper R Grimsley, George S Barron, Edwin Barnes, Sophia E Economou, and Nicholas J Mayhall. Adaptive, problem-tailored variational quantum eigensolver mitigates rough parameter landscapes and barren plateaus. npj Quantum Information, 9(1):19, 2023. 1
- [28] Geoffrey Hinton. Neural networks for machine learning, lecture 6a, overview of mini-batch gradient descent, 2012. URL http://www.cs.toronto.edu/~tijmen/csc321/slides/lecture_slides_lec6.pdf. 4
- [29] Kurt Hornik, Maxwell Stinchcombe, and Halbert White. Multilayer feedforward networks are universal approximators. *Neural networks*, 2(5):359–366, 1989. 2, 3

- [30] Jerry Yao-Chieh Hu, Pei-Hsuan Chang, Robin Luo, Hong-Yu Chen, Weijian Li, Wei-Po Wang, and Han Liu. Outlier-efficient hopfield layers for large transformerbased models. arXiv preprint arXiv:2404.03828, 2024. 12
- [31] Jerry Yao-Chieh Hu, Weimin Wu, Zhuoru Li, Zhao Song, and Han Liu. On statistical rates and provably efficient criteria of latent diffusion transformers (dits). arXiv preprint arXiv:2407.01079, 2024. 12
- [32] Jiaqi Hu, Junning Li, Yanling Lin, Hanlin Long, Xu-Sheng Xu, Zhaofeng Su, Wengang Zhang, Yikang Zhu, and Man-Hong Yung. Benchmarking variational quantum eigensolvers for quantum chemistry. arXiv preprint arXiv:2211.12775, 2022. 6
- [33] Matteo Ippoliti, Kostyantyn Kechedzhi, Roderich Moessner, S.L. Sondhi, and Vedika Khemani. Many-body physics in the nisq era: Quantum programming a discrete time crystal. PRX Quantum, 2:030346, Sep 2021.
- [34] Nishant Jain, Brian Coyle, Elham Kashefi, and Niraj Kumar. Graph neural network initialisation of quantum approximate optimisation. *Quantum*, 6:861, November 2022. ISSN 2521-327X. 3
- [35] Abhinav Kandala, Antonio Mezzacapo, Kristan Temme, Maika Takita, Markus Brink, Jerry M Chow, and Jay M Gambetta. Hardware-efficient variational quantum eigensolver for small molecules and quantum magnets. *nature*, 549(7671):242–246, 2017. 6
- [36] Diederik P. Kingma and Jimmy Ba. Adam: A method for stochastic optimization, 2017. 4
- [37] Bálint Koczor and Simon C. Benjamin. Quantum analytic descent. *Physical Review Research*, 4(2), April 2022. ISSN 2643-1564.
- [38] Ankit Kulshrestha, Xiaoyuan Liu, Hayato Ushijima-Mwesigwa, and Ilya Safro. Learning to optimize quantum neural network without gradients, 2023, 13
- [39] Xinwei Lee, Yoshiyuki Saito, Dongsheng Cai, and Nobuyoshi Asai. Parameters fixing strategy for quantum approximate optimization algorithm. In 2021 IEEE International Conference on Quantum Computing and Engineering (QCE). IEEE, October 2021. 3
- [40] Xia Liu, Geng Liu, Jiaxin Huang, Hao-Kai Zhang, and Xin Wang. Mitigating barren plateaus of variational quantum eigensolvers, 2022. 1
- [41] Owen Lockwood. Optimizing quantum variational circuits with deep reinforcement learning, 2022. 13
- [42] Haozheng Luo, Jiahao Yu, Wenxin Zhang, Jialong Li, Jerry Yao-Chieh Hu, Xinyu Xing, and Han Liu. Decoupled alignment for robust plug-and-play adaptation, 2024. URL https://arxiv.org/abs/2406.01514. 12
- [43] Alicia B. Magann, Kenneth M. Rudinger, Matthew D. Grace, and Mohan Sarovar. Feedback-based quantum optimization. *Physical Review Letters*, 129(25), December 2022. ISSN 1079-7114. 1
- [44] Andrea Mari, Thomas R. Bromley, Josh Izaac, Maria Schuld, and Nathan Killoran. Transfer learning in hybrid classical-quantum neural networks. *Quantum*, 4:340, October 2020. ISSN 2521-327X. 12
- [45] S. Marsh and J. B. Wang. Combinatorial optimization via highly efficient quantum walks. *Phys. Rev. Res.*, 2: 023302, Jun 2020. 1
- [46] Sam McArdle, Suguru Endo, Alán Aspuru-Guzik, Simon C. Benjamin, and Xiao Yuan. Quantum computational chemistry. Reviews of Modern Physics, 92(1), March 2020. ISSN 1539-0756.

- [47] Jarrod R McClean, Sergio Boixo, Vadim N Smelyanskiy, Ryan Babbush, and Hartmut Neven. Barren plateaus in quantum neural network training landscapes. *Nature communications*, 9(1):4812, 2018. 1, 3, 5
- [48] Luke Metz, Niru Maheswaranathan, Jeremy Nixon, C. Daniel Freeman, and Jascha Sohl-Dickstein. Understanding and correcting pathologies in the training of learned optimizers, 2019. 4, 12, 14
- [49] Luke Metz, C Daniel Freeman, James Harrison, Niru Maheswaranathan, and Jascha Sohl-Dickstein. Practical tradeoffs between memory, compute, and performance in learned optimizers. In Conference on Lifetong Learning Agents, pages 142–164. PMLR, 2022. 14
- [50] Luke Metz, James Harrison, C. Daniel Freeman, Amil Merchant, Lucas Beyer, James Bradbury, Naman Agrawal, Ben Poole, Igor Mordatch, Adam Roberts, and Jascha Sohl-Dickstein. Velo: Training versatile learned optimizers by scaling up, 2022. 13, 14
- [51] Peter JJ O'Malley, Ryan Babbush, Ian D Kivlichan, Jonathan Romero, Jarrod R McClean, Rami Barends, Julian Kelly, Pedram Roushan, Andrew Tranter, Nan Ding, et al. Scalable quantum simulation of molecular energies. *Physical Review X*, 6(3):031007, 2016. 6
- [52] Alberto Peruzzo, Jarrod McClean, Peter Shadbolt, Man-Hong Yung, Xiao-Qi Zhou, Peter J. Love, Alán Aspuru-Guzik, and Jeremy L. O'Brien. A variational eigenvalue solver on a photonic quantum processor. *Nature Com*munications, 5(1), July 2014. ISSN 2041-1723. 5, 6
- [53] Kyle Poland, Kerstin Beer, and Tobias J. Osborne. No free lunch for quantum machine learning, 2020. 2
- [54] John Preskill. Reliable quantum computers. Proceedings of the Royal Society of London. Series A: Mathematical, Physical and Engineering Sciences, 454(1969):385–410, January 1998. ISSN 1471-2946.
- [55] John Preskill. Quantum computing in the nisq era and beyond. Quantum, 2:79, 2018. 1
- [56] Simon J.D. Prince. Understanding Deep Learning. The MIT Press, 2023. URL http://udlbook.com. 12
- [57] Adrián Pérez-Salinas, Alba Cervera-Lierta, Elies Gil-Fuster, and José I. Latorre. Data re-uploading for a universal quantum classifier. *Quantum*, 4:226, February 2020. ISSN 2521-327X. 5, 11, 12, 13
- [58] Mirco Ravanelli, Titouan Parcollet, Peter Plantinga, Aku Rouhe, Samuele Cornell, Loren Lugosch, Cem Subakan, Nauman Dawalatabad, Abdelwahab Heba, Jianyuan Zhong, et al. Speechbrain: A general-purpose speech toolkit. arXiv preprint arXiv:2106.04624, 2021. 12
- [59] Alex Daniel Reneau, Jerry Yao-Chieh Hu, Ammar Gilani, and Han Liu. Feature programming for multivariate time series prediction. In *International Conference* on Machine Learning, pages 29009–29029. PMLR, 2023.
- [60] David E Rumelhart, Geoffrey E Hinton, and Ronald J Williams. Learning representations by back-propagating errors. nature, 323(6088):533–536, 1986. 4
- [61] Robin M. Schmidt, Frank Schneider, and Philipp Hennig. Descending through a crowded valley - benchmarking deep learning optimizers, 2021. 4
- [62] Maria Schuld and Nathan Killoran. Is quantum advantage the right goal for quantum machine learning? PRX Quantum, 3(3), July 2022. ISSN 2691-3399. 10
- [63] Maria Schuld, Ville Bergholm, Christian Gogolin, Josh Izaac, and Nathan Killoran. Evaluating analytic gradients on quantum hardware. *Physical Review A*, 99(3):

- 032331, 2019. 1
- [64] Maria Schuld, Alex Bocharov, Krysta M. Svore, and Nathan Wiebe. Circuit-centric quantum classifiers. *Physical Review A*, 101(3), March 2020. ISSN 2469-9934.
- [65] David Sherrington and Scott Kirkpatrick. Solvable model of a spin-glass. *Physical review letters*, 35(26):1792, 1975.
- [66] Peter W. Shor. Polynomial-time algorithms for prime factorization and discrete logarithms on a quantum computer. SIAM Journal on Computing, 26(5):1484–1509, October 1997. ISSN 1095-7111.
- [67] Siddharth Srivastava and Gaurav Sharma. Omnivec: Learning robust representations with cross modal sharing, 2023. 12
- [68] James Stokes, Josh Izaac, Nathan Killoran, and Giuseppe Carleo. Quantum natural gradient. Quantum, 4:269, May 2020. ISSN 2521-327X. 1, 3, 4, 5, 8
- [69] Jiace Sun, Lixue Cheng, and Weitang Li. Toward chemical accuracy with shallow quantum circuits: A clifford-based hamiltonian engineering approach. *Journal of Chemical Theory and Computation*, 20(2):695–707, 2024.
- [70] Gemini Team, Rohan Anil, Sebastian Borgeaud, Yonghui Wu, Jean-Baptiste Alayrac, Jiahui Yu, Radu Soricut, Johan Schalkwyk, Andrew M Dai, Anja Hauth, et al. Gemini: a family of highly capable multimodal models. arXiv preprint arXiv:2312.11805, 2023. 12
- [71] Guillaume Verdon, Michael Broughton, Jarrod R. Mc-Clean, Kevin J. Sung, Ryan Babbush, Zhang Jiang, Hartmut Neven, and Masoud Mohseni. Learning to learn with quantum neural networks via classical neural networks, 2019. 2, 12, 13
- [72] Olga Wichrowska, Niru Maheswaranathan, Matthew W Hoffman, Sergio Gomez Colmenarejo, Misha Denil, Nando Freitas, and Jascha Sohl-Dickstein. Learned optimizers that scale and generalize. In *International con*ference on machine learning, pages 3751–3760. PMLR, 2017. 14
- [73] Max Wilson, Sam Stromswold, Filip Wudarski, Stuart Hadfield, Norm M. Tubman, and Eleanor Rieffel. Optimizing quantum heuristics with meta-learning, 2019. 2, 12, 13
- [74] Dennis Wu, Jerry Yao-Chieh Hu, Weijian Li, Bo-Yu Chen, and Han Liu. STanhop: Sparse tandem hopfield model for memory-enhanced time series prediction. In The Twelfth International Conference on Learning Representations, 2024. 12
- [75] Chenwei Xu, Jerry Yao-Chieh Hu, Aakaash Narayanan, Mattson Thieme, Vladimir Nagaslaev, Mark Austin, Jeremy Arnold, Jose Berlioz, Pierrick Hanlet, Aisha Ibrahim, et al. Beyond pid controllers: Ppo with neuralized pid policy for proton beam intensity control in mu2e. arXiv preprint arXiv:2312.17372, 2023. 12
- [76] Chenwei Xu, Yu-Chao Huang, Jerry Yao-Chieh Hu, Weijian Li, Ammar Gilani, Hsi-Sheng Goan, and Han Liu. BiSHop: Bi-directional cellular learning for tabular data with generalized sparse modern hopfield model. In Forty-first International Conference on Machine Learning, 2024. 12
- [77] Jiahao Yu, Haozheng Luo, Jerry Yao-Chieh Hu, Wenbo Guo, Han Liu, and Xinyu Xing. Enhancing jailbreak attack against large language models through silent tokens, 2024. URL https://arxiv.org/abs/2405.20653. 12

- [78] Ailing Zeng, Muxi Chen, Lei Zhang, and Qiang Xu. Are transformers effective for time series forecasting? In *Proceedings of the AAAI conference on artificial intelligence*, volume 37, pages 11121–11128, 2023. 12
- [79] Kaining Zhang, Liu Liu, Min-Hsiu Hsieh, and Dacheng Tao. Escaping from the barren plateau via gaussian initializations in deep variational quantum circuits. Advances in Neural Information Processing Systems, 35: 18612–18627, 2022. 1
- [80] Yu Zhang, Wei Han, James Qin, Yongqiang Wang, Ankur Bapna, Zhehuai Chen, Nanxin Chen, Bo Li, Vera Axelrod, Gary Wang, et al. Google usm: Scaling automatic speech recognition beyond 100 languages. arXiv preprint arXiv:2303.01037, 2023. 12
- [81] Zhi Zhang, Weijian Li, and Han Liu. Multivariate time series forecasting by graph attention networks with theoretical guarantees. In *International Conference on Artifi*cial Intelligence and Statistics, pages 2845–2853. PMLR, 2024. 12
- [82] Zhihan Zhou, Yanrong Ji, Weijian Li, Pratik Dutta, Ramana Davuluri, and Han Liu. Dnabert-2: Efficient foundation model and benchmark for multi-species genome. arXiv preprint arXiv:2306.15006, 2023. 12
- [83] Zhihan Zhou, Weimin Wu, Harrison Ho, Jiayi Wang, Lizhen Shi, Ramana V Davuluri, Zhong Wang, and Han Liu. Dnabert-s: Learning species-aware dna embedding with genome foundation models. ArXiv, 2024. 12

 $\ensuremath{\mathsf{TABLE}}$ III: Default Hyperparameters for Baseline Optimizers.

Optimizer	Default lr	Default Values
Adam	0.01	$\beta_1 = 0.9, \beta_2 = 0.999, \epsilon = 10^{-8}$ $\epsilon = 10^{-8}$
Adagrad RMSprop	0.01	$\epsilon = 10^{-6}$ $\rho = 0.9, \epsilon = 10^{-8}$
Momentum		m = 0.9
Vanilla GD	0.0-	N/A
Vanilla GD QNGD	0.01 0.01	$N/A \\ \lambda = 0.01$

Appendix C: Version Information

 $\ensuremath{\mathsf{TABLE}}$ IV: Software and System Information.

Software	Version	
pennylane	0.34.0	
wandb	0.16.3	
tqdm	4.66.2	
scikit-learn	1.4.1.post1	
matplotlib	3.8.3	
torch	4.66.2	
torchvision	0.17.2	
torchaudio	0.10.0 + rocm 4.1	
h5py	3.10.0	
fsspec	2024.2.0	
aiohttp	3.9.3	
Parameter	Value	
Python version	3.9.18	
Python compiler	GCC 11.2.0	
Python build	main, Sep 11 2023 13:41:44	
OS	Linux	
CPUs	40	
CPUs Memory (GB)	754	
GPUs	4 (Tesla V100S-PCIE-32GB)	
$\mathrm{GPUs}\ \mathrm{Memory}\ (\mathrm{GB})$	128	
Fri Apr 19 03:05:51 2024 UTC		

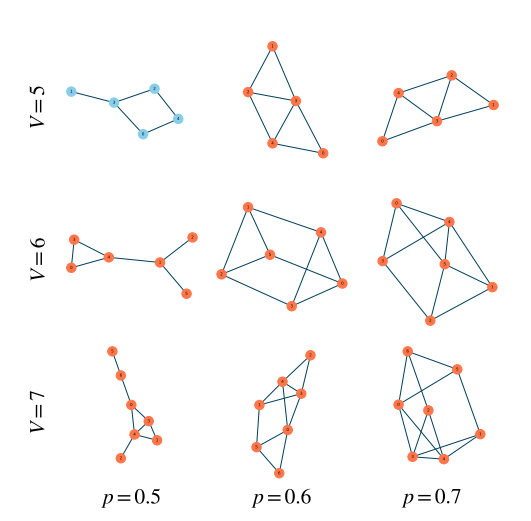


FIG. 13: Examples of Randomly Generated Erdős-Rényi $\mathcal{G}(n,p)$. We randomly generate the Erdős-Rényi graph for the MaxCut problem for vertices $V \in \{5,6,7\}$ and probability $p \in \{0.5,0.6,0.7\}$ where n is the number of vertices and each pair of n vertices connected by an edge with probability p. Horizontal direction represents different p values and vertical direction represents different values of V.